NASA Technical Memorandum 81161

Static Calibration of a Two-Dimensional Wedge Nozzle With Thrust Vectoring and Spanwise Blowing

Michael J. Harris and Michael D. Falarski

April 1980

National Aeronautics and Space Administration

NASA Technical Memorandum 81161

Static Calibration of a Two-Dimensional Wedge Nozzle With Thrust Vectoring and Spanwise Blowing

Michael J. Harris, David W. Taylor Naval Ship Research and Development Center, Bethesda, Maryland
Michael D. Falarski, NASA-Ames Research Center, Moffett Field, California

National Aeronautics and Space Administration

Ames Research Center
Moffett Field, California 94035

SYMBOLS

C_T	Thrust coefficient, $F_{g/qS}$
F_A	Measured axial force
F_g	Gross thrust, $F_P + F_{SWB}$
F_N	Measured normal force
F_P	Total force produced by a primary nozzle
F_R	Longitudinally resultant thrust, $\sqrt{(F_A)^2 + (F_N)^2}$
F_S	Measured side force
F_{SWB}	Total force produced by spanwise blowing
SWB	Spanwise blowing
TPRED	Ratio of the total pressure in the exhaust duct to ambient pressure
TPRFR	Ratio of the total pressure measured by the flap rake to ambient pressure
TPRNR	Ratio of the total pressure measured by the nozzle rake to ambient pressure
θ	Static thrust turning (vectoring) angle
Φ	Spanwise blowing sweep angle
δ_f	Flap deflection, deg

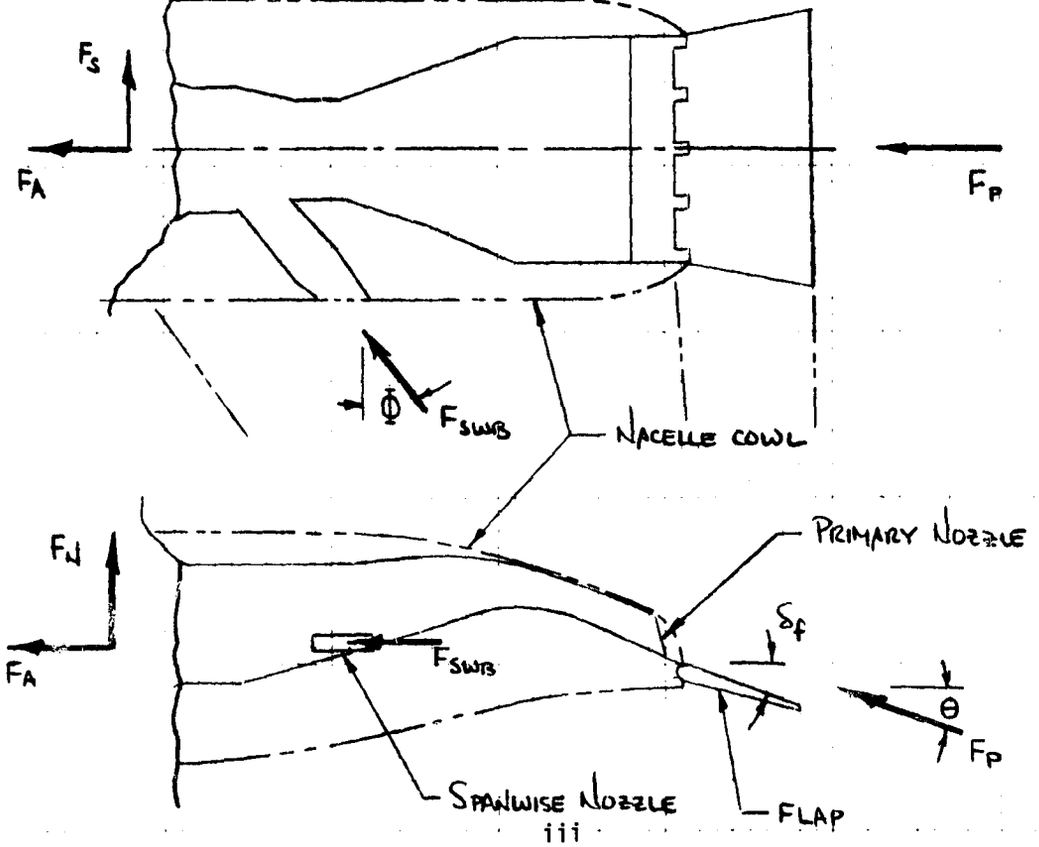

SUMMARY

The results of a static calibration of the two-dimensional wedge nozzles on a STOL configuration of a large-scale fighter model are reported here. These nozzles internally turn the efflux produced by two turbojets down 25° and exhaust it over the deflected trailing edge of the wing. This arrangement provides direct thrust lift, and enhances wing lift by producing supercirculation. Additionally, this arrangement provides thrust vectoring by varying the deflection of the wing's trailing edge. In this test the thrust was vectored from 10° to 38°.

This system was also calibrated with spanwise blowing for augmentation of the leading-edge vortex. When 16% of the turbojet efflux is blown spanwise, the thrust recovered is 92% of the thrust produced when the total efflux is exhausted longitudinally.

INTRODUCTION

In support of the investigation of a highly-maneuverable supersonic V/STOL fighter concept, a pair of two-dimensional wedge nozzles was statically calibrated at the Ames Static Test Facility. The propulsive-lift concept, for which these nozzles were designed, uses a thick, high pressure jet, typical of fighter propulsion systems, to enhance wing lift. This propulsive lift system provides the supersonic configuration with improved transonic maneuverability and STOL performance.

One such concept, termed Vectored Thrust/Supercirculation (VT/SC), is described in reference 1. Here wing lift is enhanced by vectoring the propulsive jet downward from fuselage mounted nozzles, in line with the deflected trailing edge of the wing. The momentum of the exhaust induces additional lift, due to supercirculation.

This arrangement was modified and combined with spanwise blowing to produce the Vectored-Engine-Over-Wing (VEO-Wing) concept. Here the engines are mounted over the wing with the efflux directed down over a portion of full-span plain flaps. As in the VT/SC concept, wing lift is enhanced. This arrangement also allows the thrust vectoring angle to be selected by varying the flap deflection. Additionally, in this concept a portion of the exhaust is blown spanwise for leading-edge-vortex augmentation. This simplifies the ducting required for spanwise blowing. References 2 and 3 show the potential of the VEO-wing concept for improving transonic maneuverability and STOL performance.

The highly-maneuverable supersonic V/STOL fighter concept is an extension of this technology. The performance of the VEO-wing concept is

combined with a VTOL capability and investigated in a large scale powered model. Figure 1 gives the dimensions of this research model and show it installed in the 40- by 80-Foot Wind Tunnel at Ames Research Center. This model is powered by a pair of J-97 turbojets. As tested, these jets developed 14011 (3150 lb) static thrust each at a pressure ratio of 2.7 and an exhaust gas temperature of 650°C. During STOL operations, this efflux provides the momentum which induce supercirculation.

The results of tne static calibration of the nozzles used in the STOL configuration are presented in this paper. These nozzles are not flight hardware but are intended to simulate the flight configuration during STOL operation. Results from the calibration will be used to define the range of thrust coefficients to be used in the wind tunnel. Additionally this data will be used in the reduction of the wind-tunnel data.

NOZZLE DESCRIPTION

Two configurations of the propulsive-lift system were calibrated. In one configuration the total jet efflux is exhausted longitudinally over the wing. A portion of this efflux is blown spanwise in the second configuration. In each configuration, the primary nozzles are two-dimensional, convergent-divergent, wedge nozzles, with an aspect ratio of eight at the throat cross-section (figure 2). The internal contour of tne nozzle duct has a fixed diffusion ratio of 1.09 and turns the flow down 25°. These nozzles were run in an overexpanded condition.

Cowl plates, which form the upper internal surface of each primary nozzle, fix the throat and exit areas. There are two cowl plates for each nozzle. Cowl-A fixes its throat area at 774 cm^2 (120 $in.^2$). Cowl B reduces this area by seventeen percent to 645 cm^2 (100 $in.^2$). The reduced throat nozzle, cowl B is used with spanwise blowing.

All of the nozzles terminate over the wing in line with the flap hinge. Flap deflections are accomplished by changing mounting brackets to produce nominal deflections in ten degrees increments from -20^o to 30^o. Flap deflections will be defined in this text as the measured angle from the wing chord plane to the upper surface of the flap (measured cold). Deflection of this flap due to the elevated temperature of the exhaust gas was not accounted for.

Spanwise blowing is provided (see figure 2) by ducting a portion of the exhaust from the primary nozzle duct out through a rectangular convergent nozzle in side of the duct. These aspect ratio four nozzles were mounted flush in the outboard fairings of each nacelle at 23% of the wing root chord. The nozzle centerline is 9 cm (3.57 in.) above the wing surface and directed aft 40^o so that it is directed parallel to the sweep of the leading edge of the wing (figure 2). The geometric area of the SWB nozzle is 17% of the standard primary nozzle, formed by cowl A, or 120 cm^2 (20 in.). Therefore the total geometric throat area of the combined SWB nozzle and the reduced area cowl B nozzle is equal to that of the standard cowl A nozzle alone.

TEST DESCRIPTION AND INSTRUMENTATION

The port nozzle assembly was statically tested before it was installed in the fighter model. The test setup is shown, at the Ames static test

facility in figure 3(a). This initial test served two purposes. First it served as a functional check of the assembly, and secondly as an evaluation of the static performance of an isolated propulsive unit. Information from this test was used to evaluate only the SWB flow angle (Φ) and relative changes in performance.

The total propulsive system was calibrated under installed conditions in the second static test. Here, the model without lifting surfaces (wings, etc.), was installed at the static test site. Figure 3(b) shows this installation.

Forces were measured, in both tests, by a set of three-component load cells, mounted between the model and each of the three support struts. Total pressure and temperature were measured in the exhaust duct, the nozzle exit and at the trailing edge of the flap.

The total pressure in the flow above the port flap was measured by a twelve probe pressure rake. This rake is shown installed on the model in figure 4(a). The height of this rake is 24.5 cm (10 in.). The diagram in figure 4(c) shows the relative position of the flap rake and the nozzle rake. The nozzle rake has eighteen total pressure probes which vertically span the past nozzle exit and extends above the nozzle into the free stream to a height of 13.3 cm (5.25 in.) (figure 4(b)). The rake is mounted on the flap with the probes parallel to the upper surface of the flap. The exhaust duct measuring station in both port and starboard nacelles, is directly aft of the J-97 turbojet. The measurements provide a time average of the total and static pressure and total temperature across the duct.

Testing was restricted to continuous wind condition below five knots at the model to reduce scatter in the turning data. Additionally all force data are an average of the forty-eight samples from each load cell. To eliminate any hysteresis in the data, it was taken after both increasing and decreasing power changes. There was, however, a zero shift in the side force component in the second static test, due to friction in the load cell mounts. Since the results of the initial static test, showed that the value of the side force component produced by the primary nozzle was negligible, this data is omitted.

RESULTS AND DISCUSSION

The port and starboard nozzle assemblies were calibrated independently. These nozzles were initially evaluated at each throat area with the nozzle flap removed. The system was then evaluated with the flap installed, over the range of flap deflections. Finally, spanwise blowing was added to the reduced area cowl-B primary nozzle.

Figure 5 presents the measured axial (F_A) and normal (F_N) forces for both primary nozzle areas and the combined cowl-B/spanwise blowing configuration. Forces have been corrected to standard sea-level conditions and plotted against the exhaust duct total pressure ratio (TPRED). This is the ratio of the total pressure measured at the exhaust duct measuring station to the ambient static pressure. The axial force (F_A) is defined as the force measured in the positive X-direction of the body axis system. The nominal force (F_N) is measured in the negative Z-direction.

Primary Nozzle

The gross thrust (F_g), for the port and starboard cowl-A primary nozzles operating independently is presented in figure 6. It represents the total measured static force. The gross thrust is used to evaluate the thrust coefficient (C_T,) to be used in the wind tunnel. Above an exhaust duct total pressure ratio (TPRED) of 1.6, the value of gross thrust is linear with respect to this pressure ratio. This graph will be discussed further in the section on spanwise blowing.

The static thrust turning angle (θ) is defined as:

$$\theta = \text{ARCTAN} \frac{F_N}{F_A}$$

This angle is presented in figure 7. The port primary nozzle with either cowl (A or B) produce a maximum turning of 31^o, while the starboard nozzle produces a maximum turning of 29^o. This turning is produced with an internal turning angle of 25^o.

Part of this turning beyond the nozzle angle is caused by changes in the nozzle geometry, due to the hot exhaust gas. But this does not account for the total effect. The gas was observed to continue turning downstream of the nozzle. This effect was also seen in the flap on results.

Spanwise Blowing

From figure 5, it is apparent that SWB adds no normal force to that produced by the reduced area primary nozzle. The total force produced by the SWB nozzles alone is presented in figure 8. This was calculated

from the sweep angle Φ and the change in axial force between the cowl-B nozzle alone case and the combined cowl B and SWB case:

$$F_{SWB} = \frac{\Delta F_A}{\sin \Phi}$$

The sweep angle Φ (or the angle between lateral and the direction of the efflux from the SWB nozzle) is calculated from the equation:

$$\Phi = \text{ARCTAN} \frac{\Delta F_A}{\Delta F_S}$$

where ΔF_A and ΔF_S are the difference in the axial and side forces measured in the static test of the isolated propulsive unit. This data is also given in figure 8.

The angle (Φ) varies from 34^o at an TPRED of 1.8 to a value of 30^o at a pressure ratio of 2.8. The change with pressure ratio seems to be due to the fact that the nozzle exit is flush with the nacelle, so that the exit is oblique to the underexpanded efflux. The free expansion of the jet produces this change in flow direction. Since studies such as in ref. 2 show that the effectiveness of the SWB is not highly sensitive to small changes in this angle, no attempt was made to alter this condition.

For the SWB configuration, the gross thrust (F_g) presented in figure 6, is calculated by the equation:

$$F_g = F_{SWB} + \sqrt{(F_A)^2 + (F_N)^2}$$

where the normal and axial forces are obtained from the reduced primary nozzle alone case. Here the force produced by each nozzle is added as if they had exhausted in a single direction. This does not bias the calculation of the thrust coefficient, and allows the two configurations used in the tunnel to be compared directly. This figure shows that SWB doesn't degrade the overall nozzle performance.

In figure 9, a comparison of the resultant force of these two configurations is shown. For a given value of total gross thrust, the resultant thrust produced by the spanwise blowing configuration is 92% of the resultant thrust produced with the total efflux of the turbojets exhausted longitudinally through the cowl-A primary nozzles. Here the opposing side forces produced by SWB cancel each other and account for the thrust loss. Additionally there is an effective loss in thrust turning of 3^{o} as shown in figure 7.

Performance with a Deflected Flap

The variation in the longtudinal resultant thrust of the primary nozzle (F_R) and the thrust vectoring angle (θ) with flap deflection, is presented in figure 10. Here we see that the thrust was vectored from -10^{o} to 38^{o} over the flap deflections tested. As in the case of the nozzle with the flap removed, here the thrust turning is greater than the measured flap deflection (δ_f). Again part of this over turning can probably be attributed to thermal expansion of the nozzle and flap. The difference in temperature on the surfaces causes the flap to curl. However this does not account for the 5^{o} to 6^{o} shown here.

When the flap is deflected to the value of 33^{o}, nominally, the thrust vectoring angle was increased by 8^{o}. By reducing the flap deflection, the thrust could be deflected back to vectoring angles to -10^{o}. There is, however, a related thrust loss. This thrust loss is 4% or less for vectoring angles of $\pm 10^{o}$ of the internal nozzle turning angle of 25^{o}. When the thrust is deflected back to a vectoring angle 0^{o} the thrust loss is 9%.

Typical total pressure profiles along the exhaust jet centerline at the nozzle and flap rake, are presented in figure 11. These profiles were taken at an exhaust duct pressure ratio of 2.5. The flap rake shows that the exhaust jet remained attached to the upper surface of the flap over the range of pressure ratios at each flap deflection tested. This suggests that the vectoring limit, from the standpoint of turning, may not have been reached.

Data for the nozzle rake shows little variation in the pressure profile due to the flap. The average flap rake pressure is plotted against the exhaust duct pressure ratio in figure 12. This represents the loss in total pressure through the exhaust duct and primary nozzle. The total pressure at the nozzle exit, with an exhaust mach number of 1.0, is 91% of the total pressure measured at the exhaust duct measuring station. As stated earlier the exhaust ducts and nozzles are not flight hardware and are not optimized for use with the J-97 turbojet. They are intended only to be used in studying the propulsion induced effects of the V/STOL fighter model.

Concluding Remarks

A pair of two-dimensional wedge nozzles was statically calibrated, with thrust vectoring and spanwise blowing. This test was conducted in connection with the investigation of the highly-maneuverable supersonic V/STOL fighter model. During the calibration the propulsive jet was vectored from -10^{o} to 38^{o}. For values of thrust vectoring of $\pm 10^{o}$ of the nozzle contour angle the thrust loss is 4% or less. The thrust recovered, with 16% of the exhaust blown spanwise, is 92% of the thrust produced with the total efflux exhausted longitudinally.

References

1. Capone, F. J.: "A Summary of Experimental Research on Propulsive-Lift Concepts in the Langley 16Foot Transonic Tunnel", AIAA Paper No. 75-1315, September 1975.

2. Woodrey, R. W.; Whitten, P. D.; Smith, C. W., and Bradley, R. G.: "An Experimental Investigation of a Vectored-Engine-Over-Wing Powered Lift Concept", Volume I, AFFDA-TR-76-92, September 1976.

3. Whitten, P. D.: "An Experimental Investigation of a Vectored-Engine-Over-Wing Powered-Lift Concept, Volume II, AFFDL-TR-76-92, March 1978.

(a) Installed in wind tunnel.

Figure 1.- V/STOL fighter model.

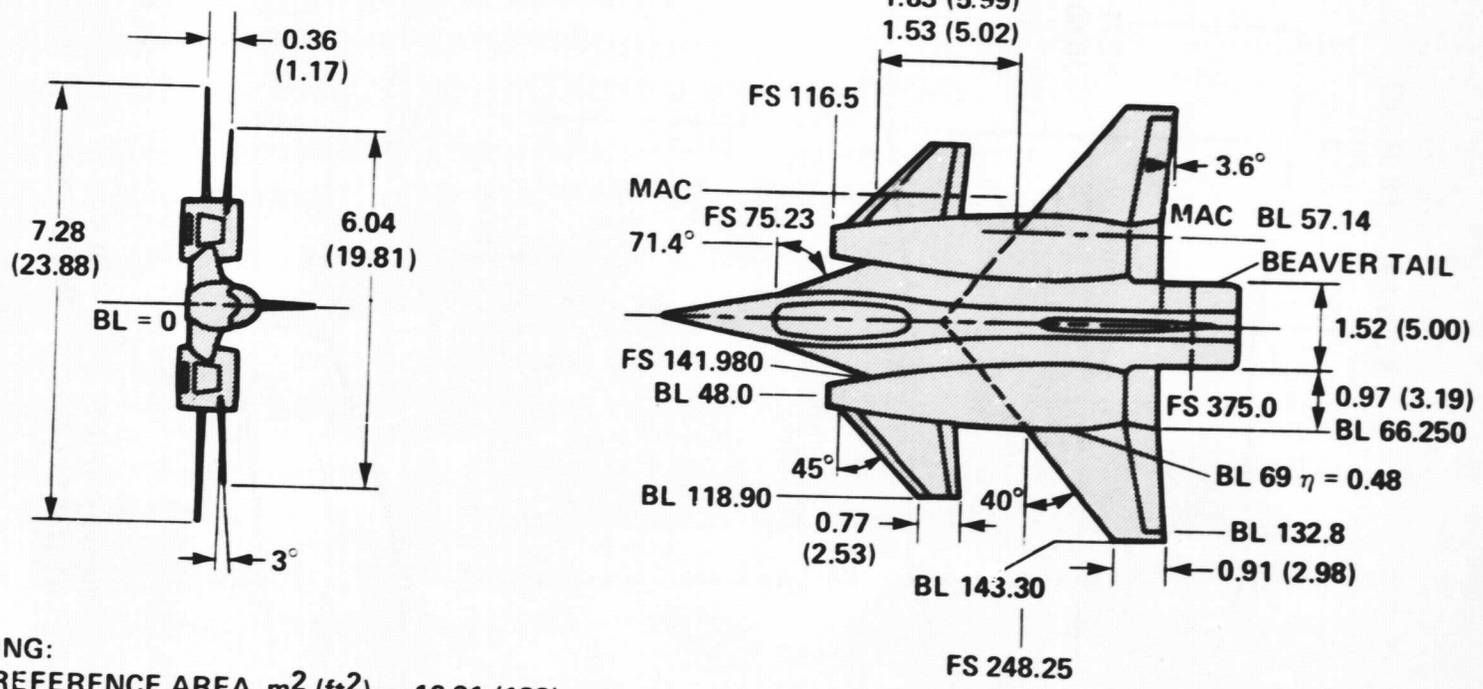

ALL DIMENSIONS IN m (ft)

WING:	
REFERENCE AREA, m^2 (ft^2)	16.91 (182)
ASPECT RATIO	3.13
TAPER RATIO	0.243
AIRFOIL SECTION	64A204
GEOMETRIC TWIST	4°
MEAN AERO CHORD, m (ft)	2.61 (8.56)
CANARD:	
AREA, m^2 (ft^2)	3.53 (37.98)
CANARD AREA/WING AREA	0.208
ASPECT RATIO	2.07
TAPER RATIO	0.419
AIRFOIL SECTION	64A004
MEAN AERO CHORD, m (ft)	1.38 (4.52)

(b) Model geometry.

Figure 1.- Concluded.

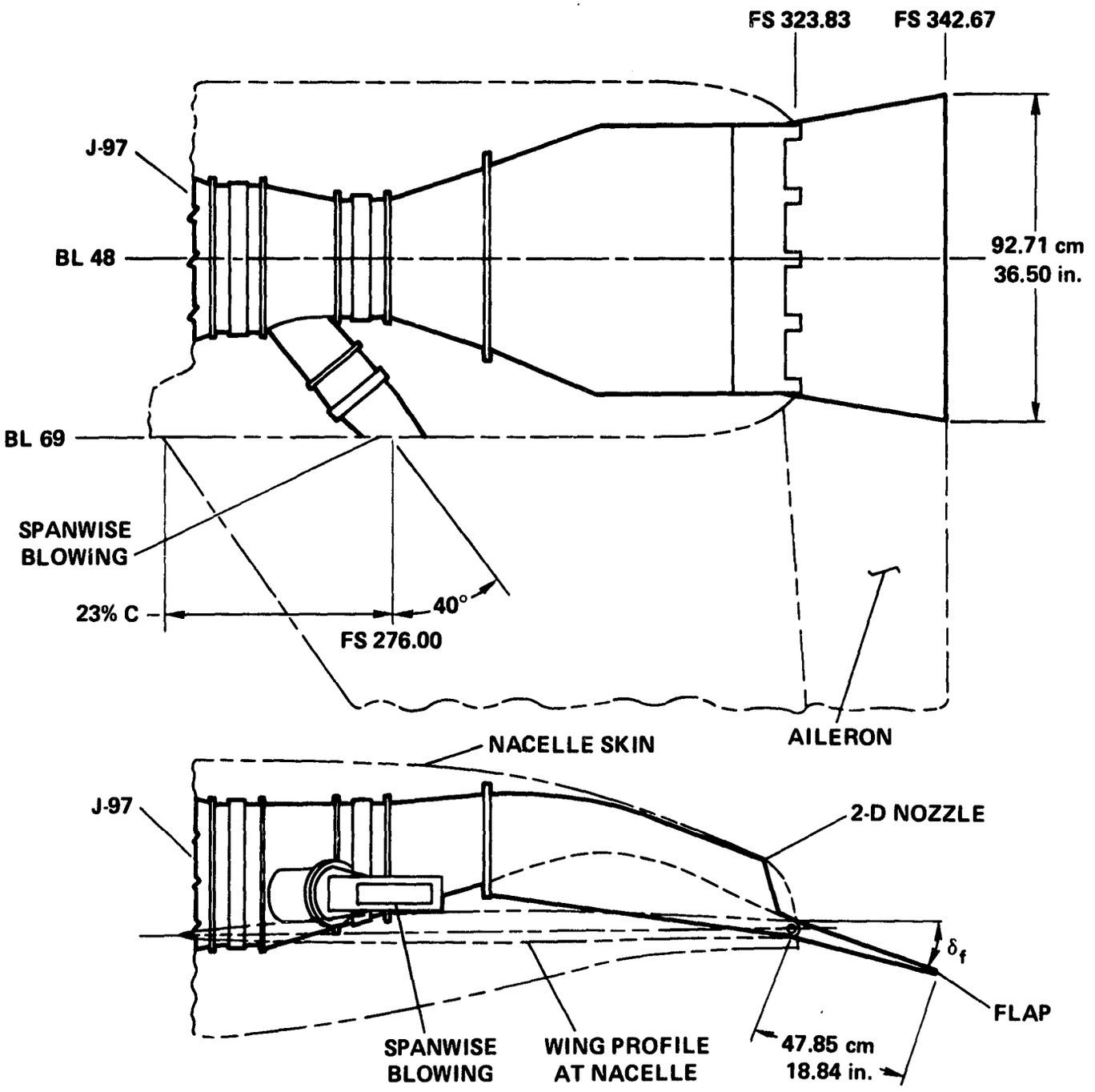

Figure 2.- Port nozzle assembly geometry.

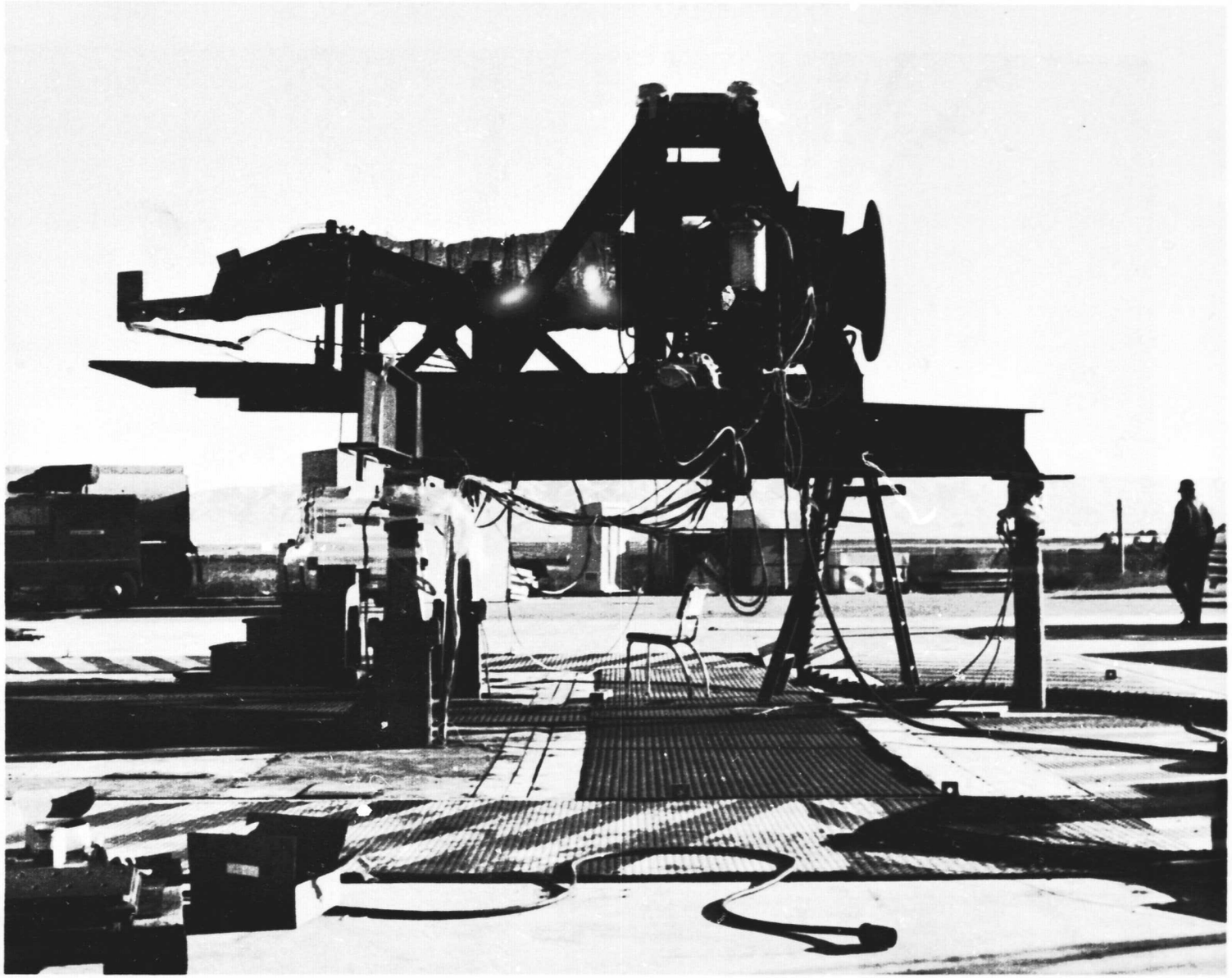

(a) Calibration of an isolated propulsive unit.

Figure 3.- Static test installation.

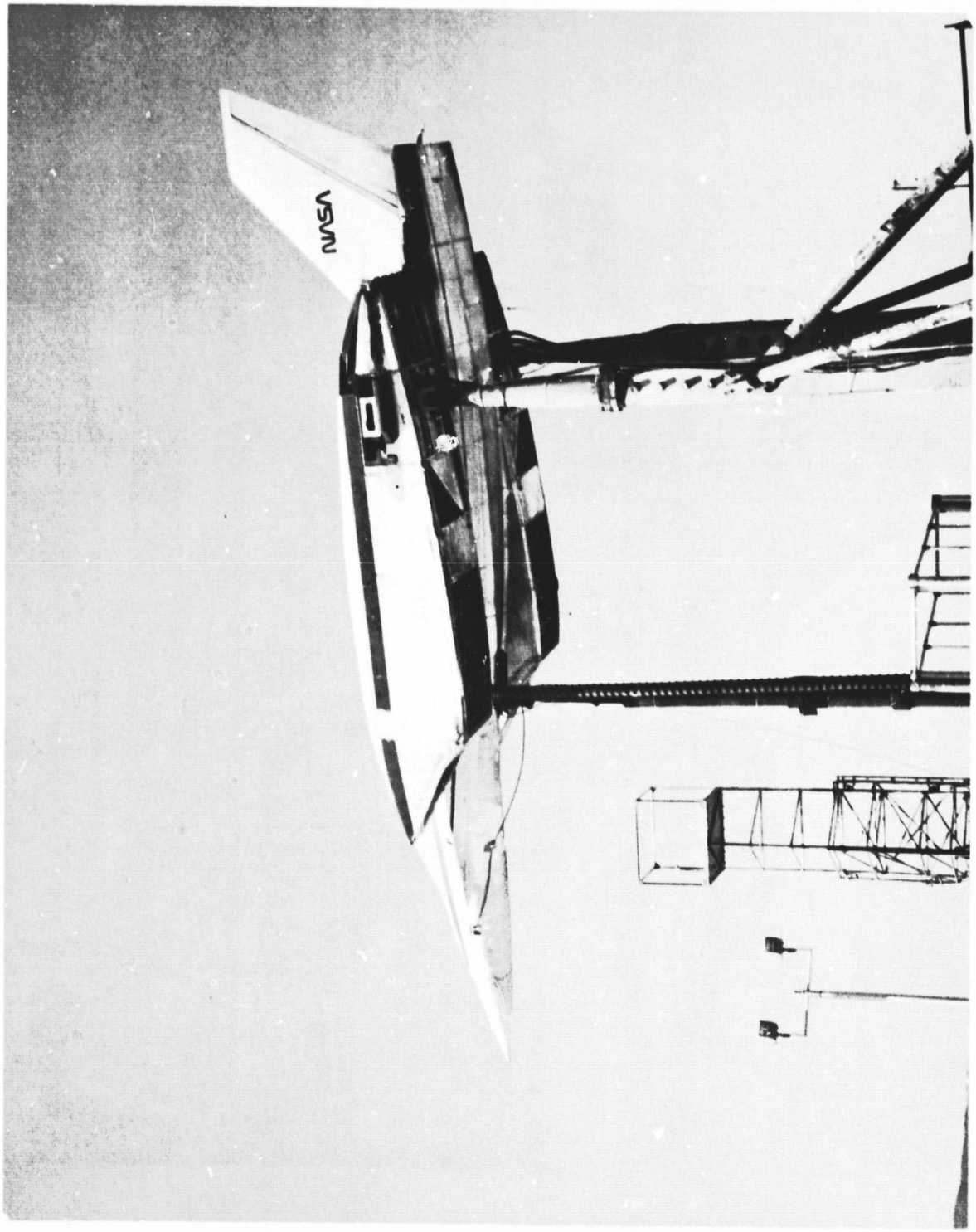

(b) Calibration of the installed propulsive system.

Figure 3.- Concluded.

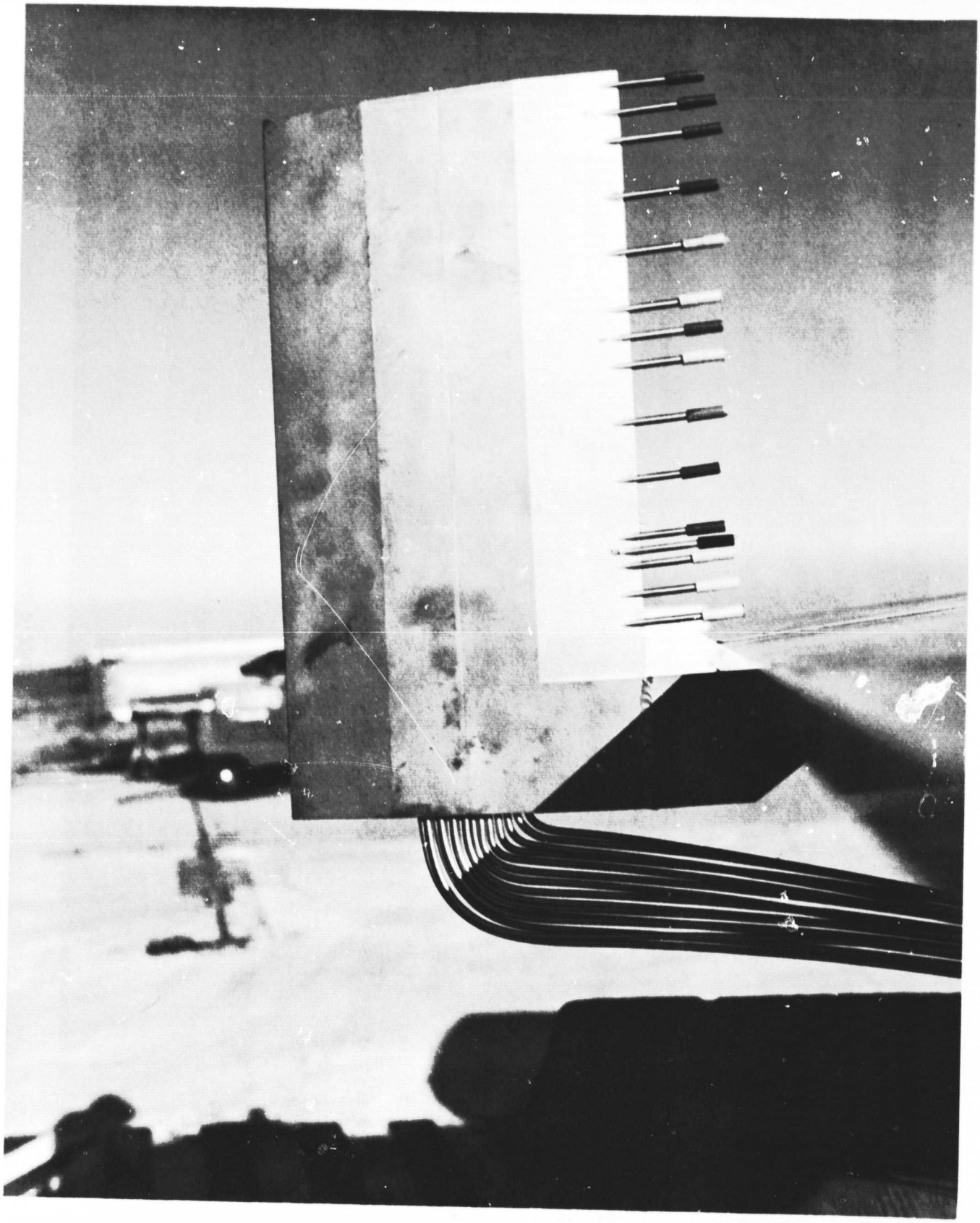

(a) Flap rake.

Figure 4.- Rakes.

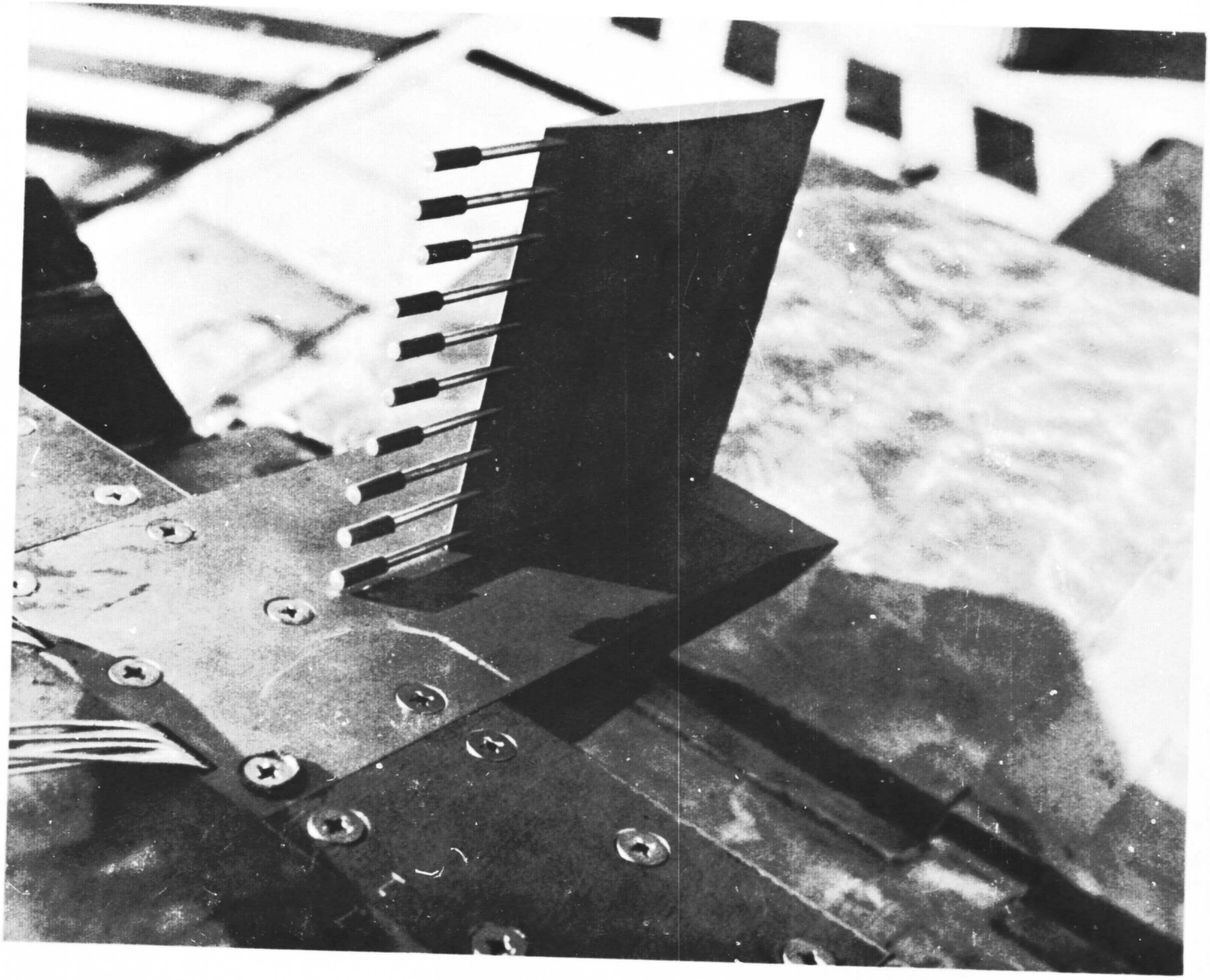

(b) Nozzle rake.

Figure 4.- Continues.

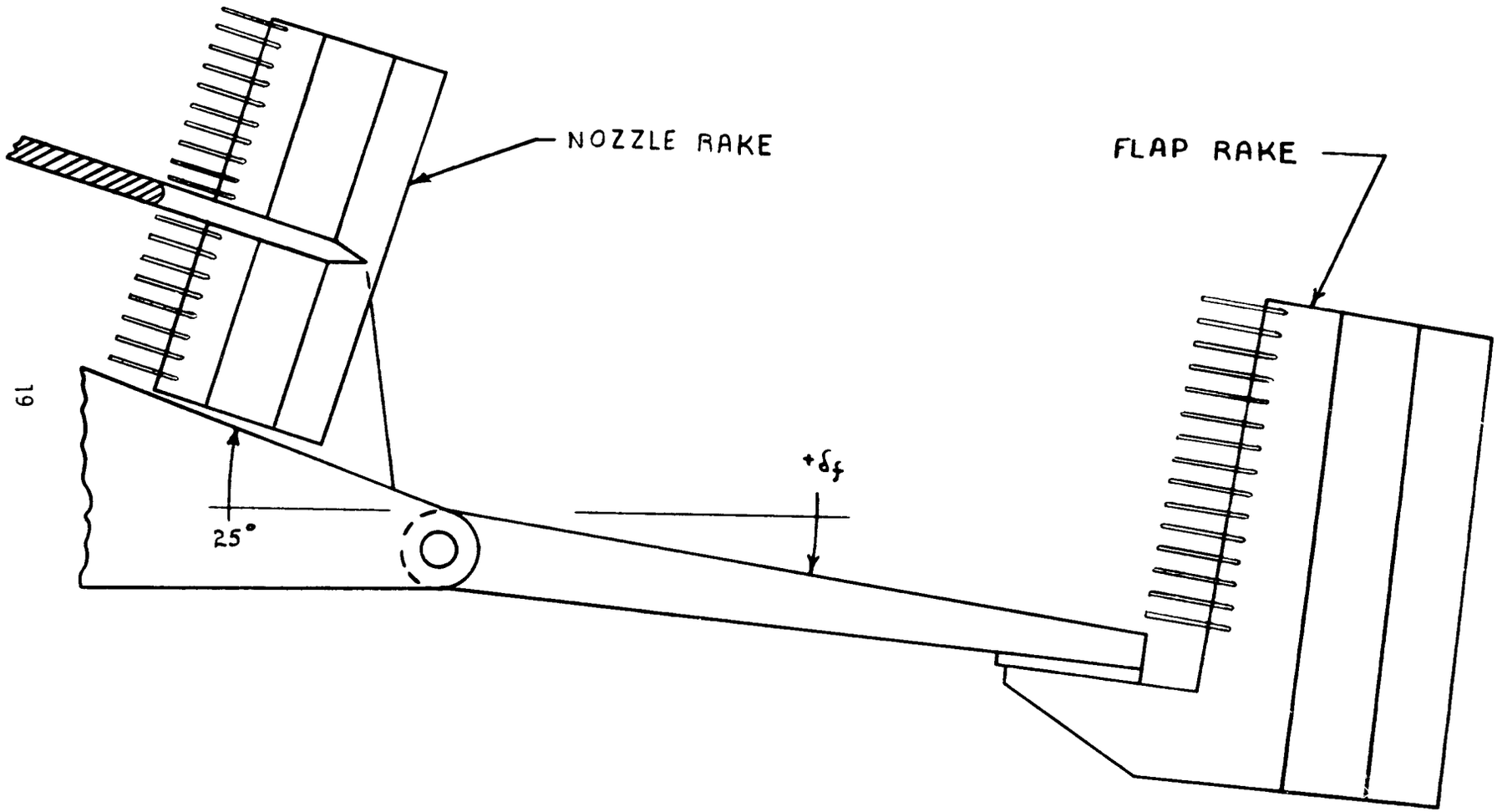

(c) RAKE INSTALLATION

FIGURE 4. CONCLUDED

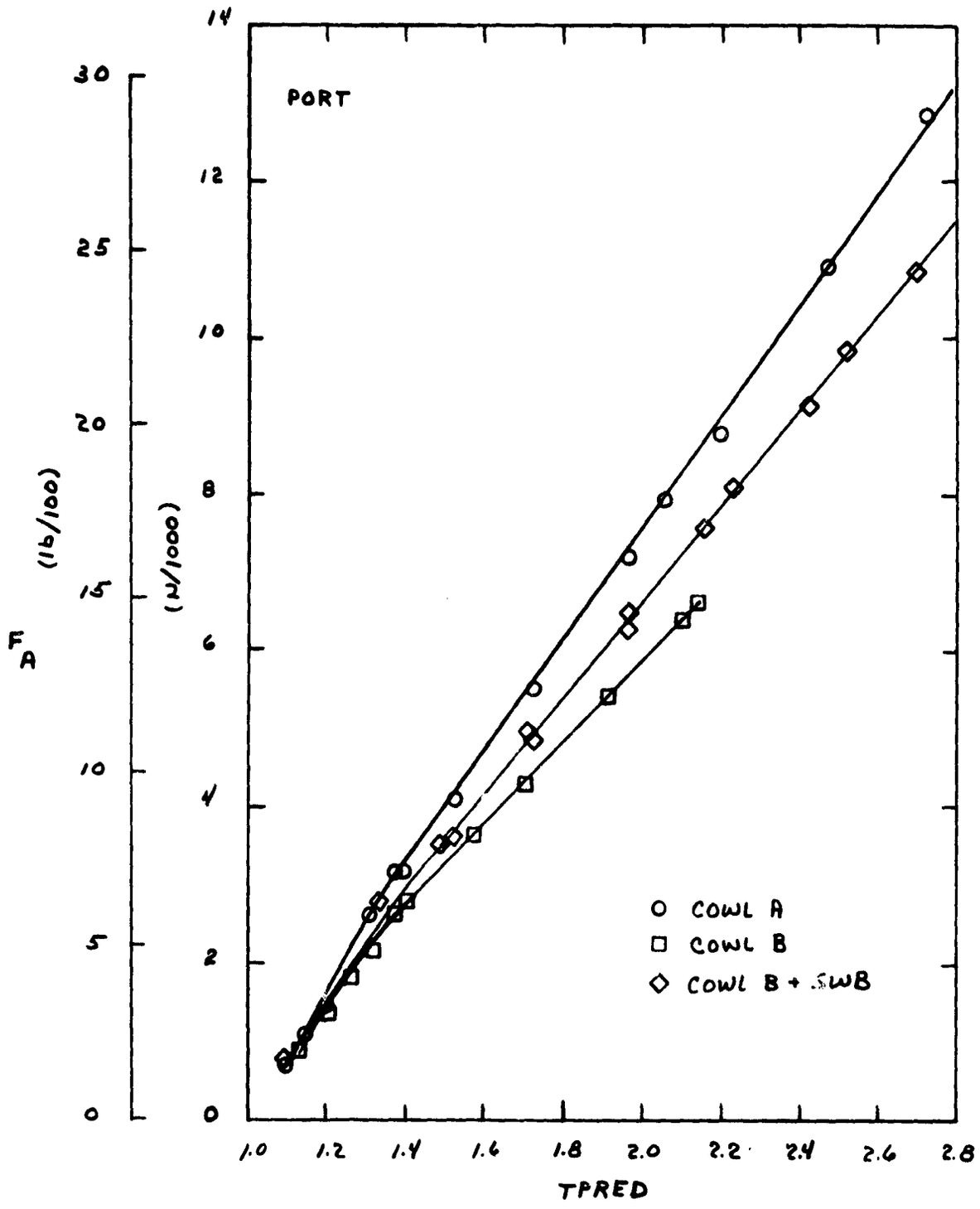

(a) AXIAL FORCE - PORT ENGINE ONLY
(NO FLAP)

FIGURE 5. MEASURED FORCES

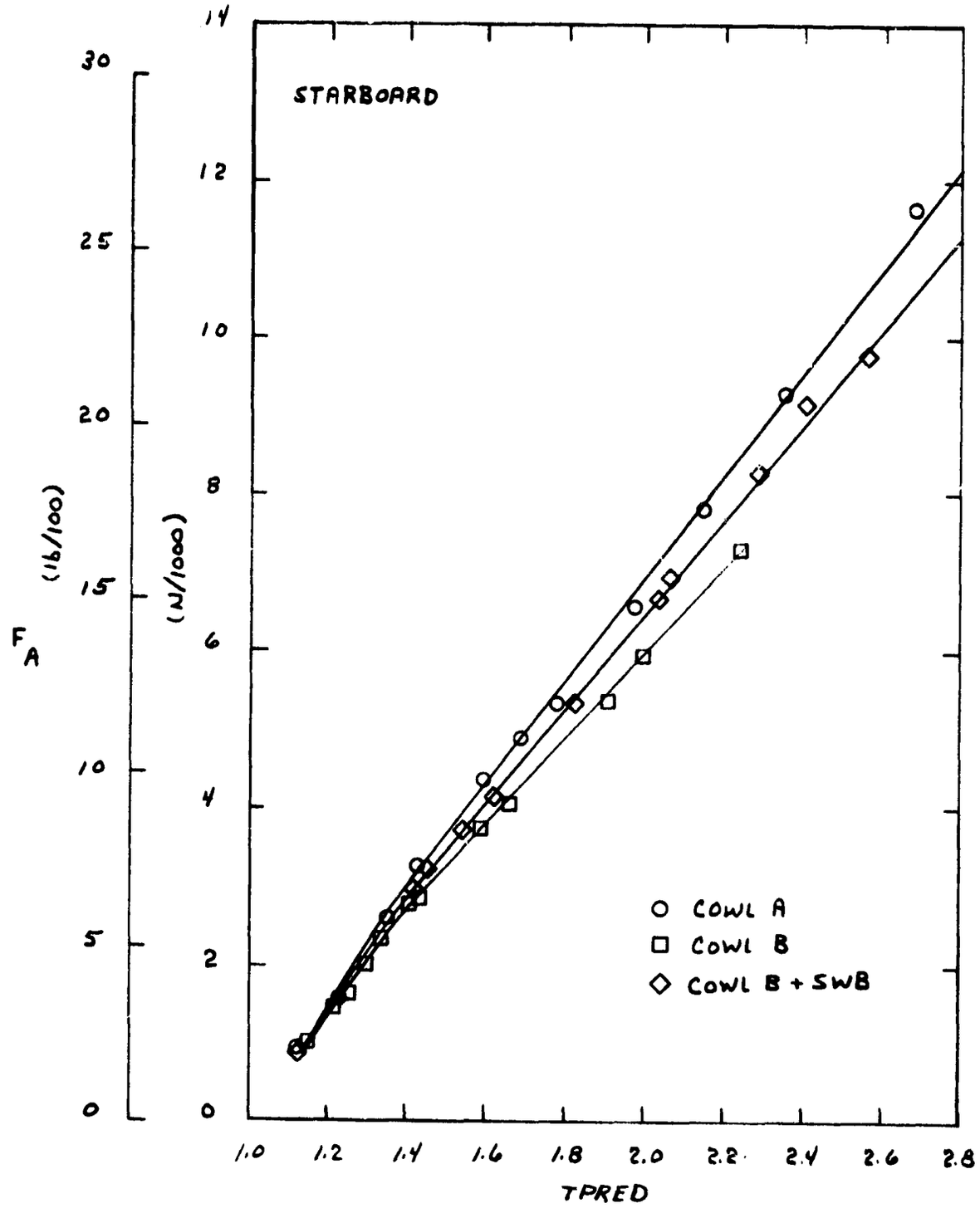

(b) AXIAL FORCE - STARBOARD ENGINE ONLY
(NO FLAP)

FIGURE 5. CONTINUES

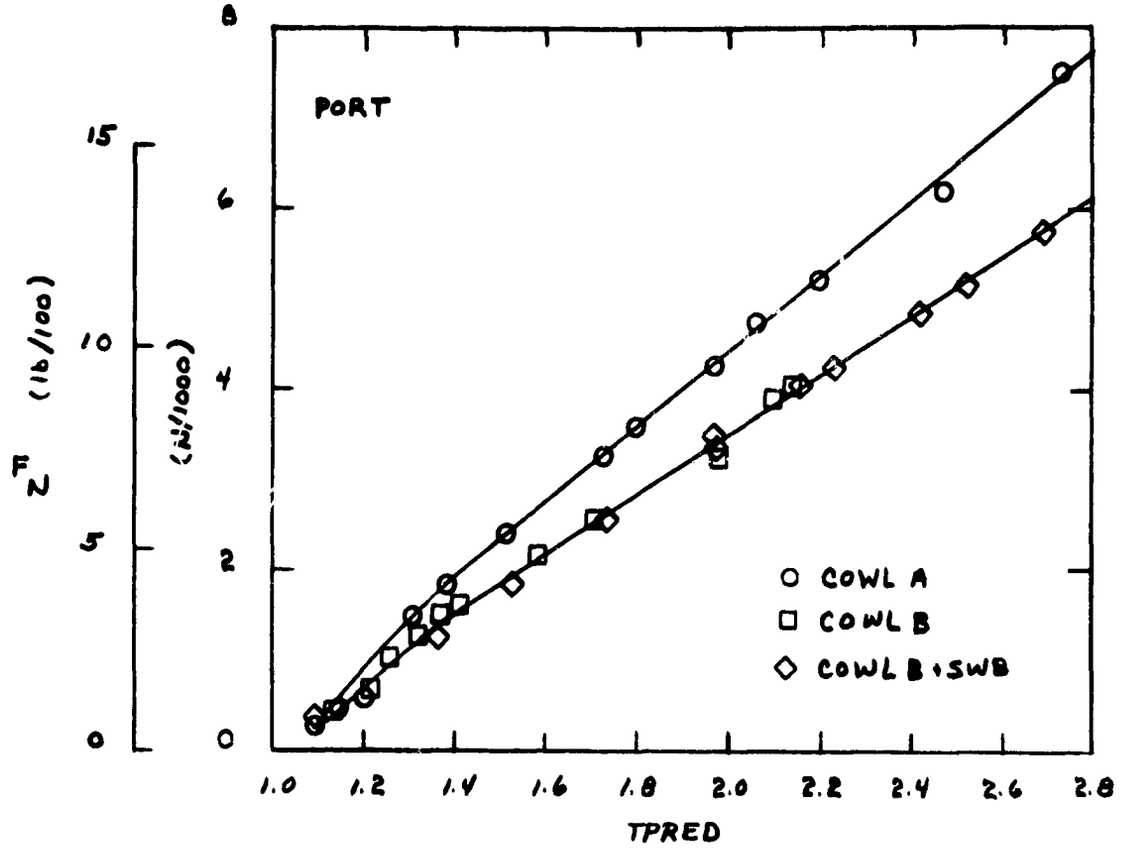

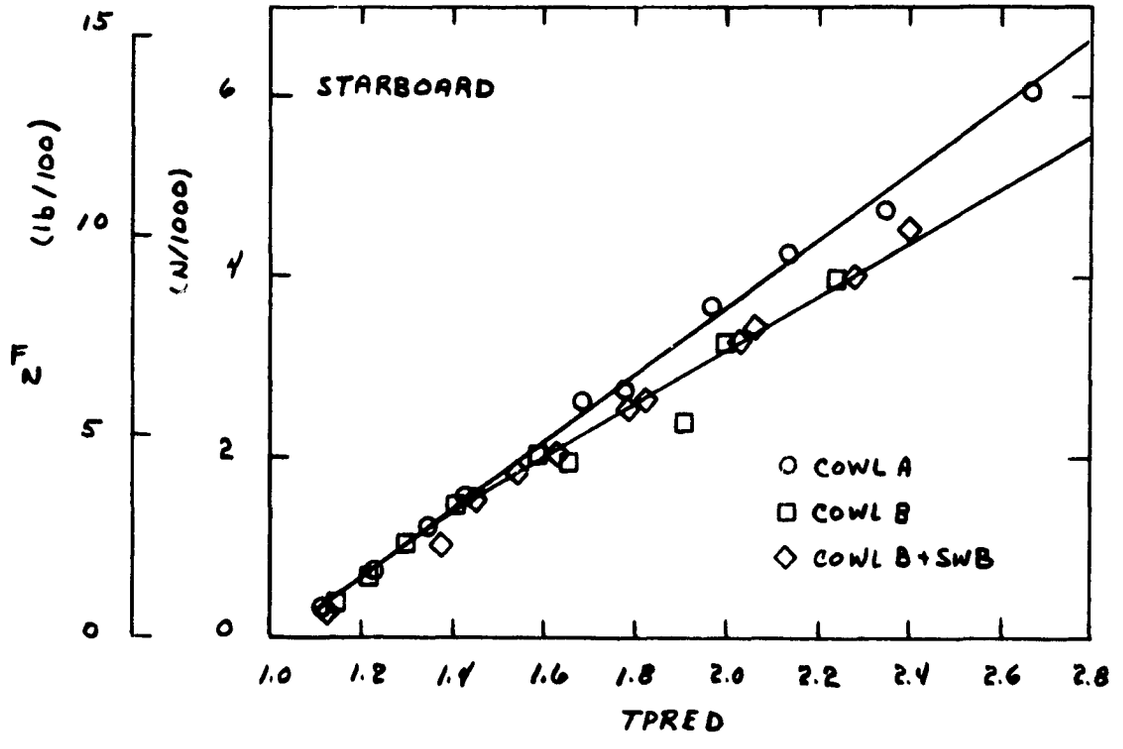

(c) NORMAL FORCE (NO FLAP)

FIGURE 5. CONCLUDED

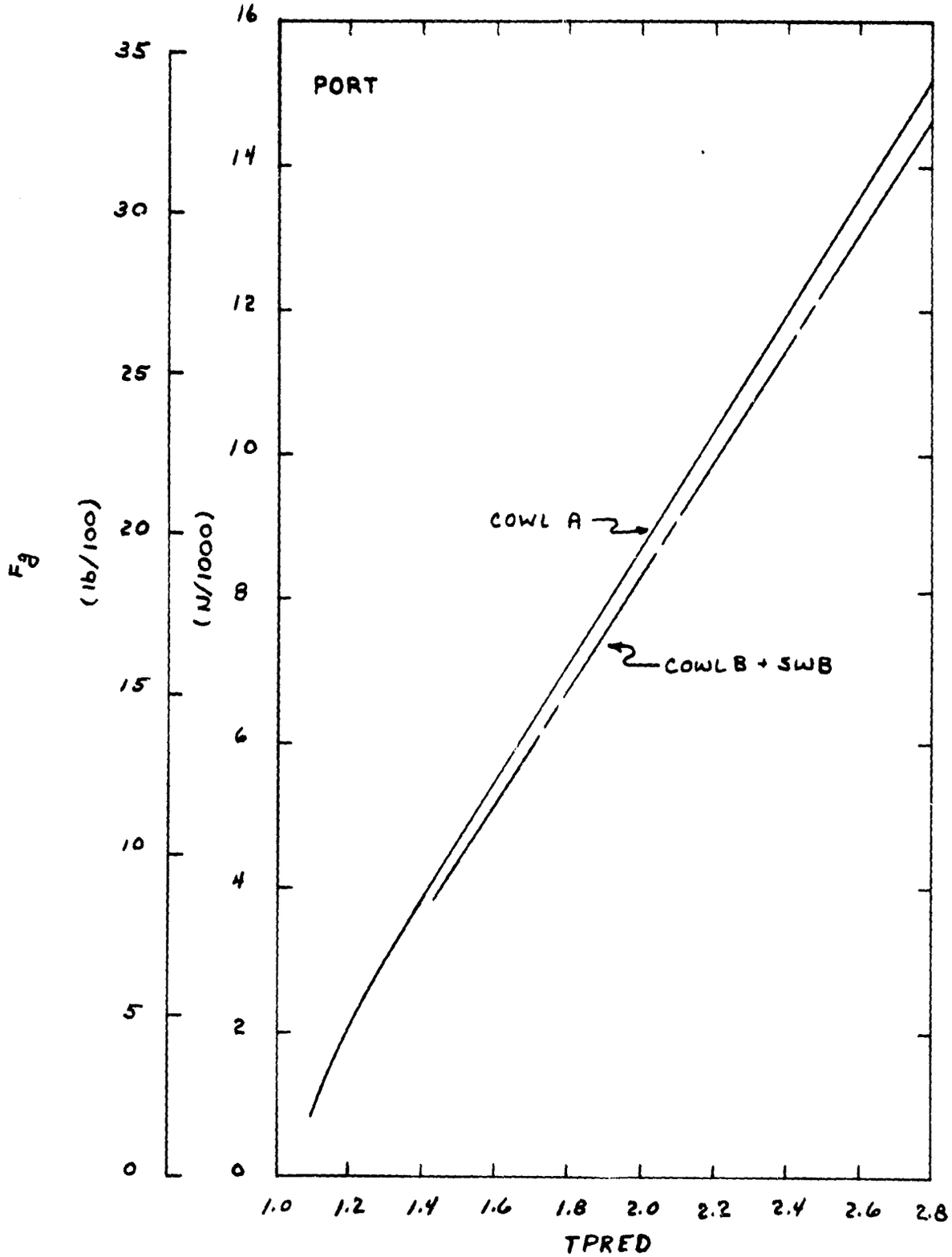

(a) PORT ENGINE ONLY

FIGURE 6. GROSS THRUST (NO FLAP)

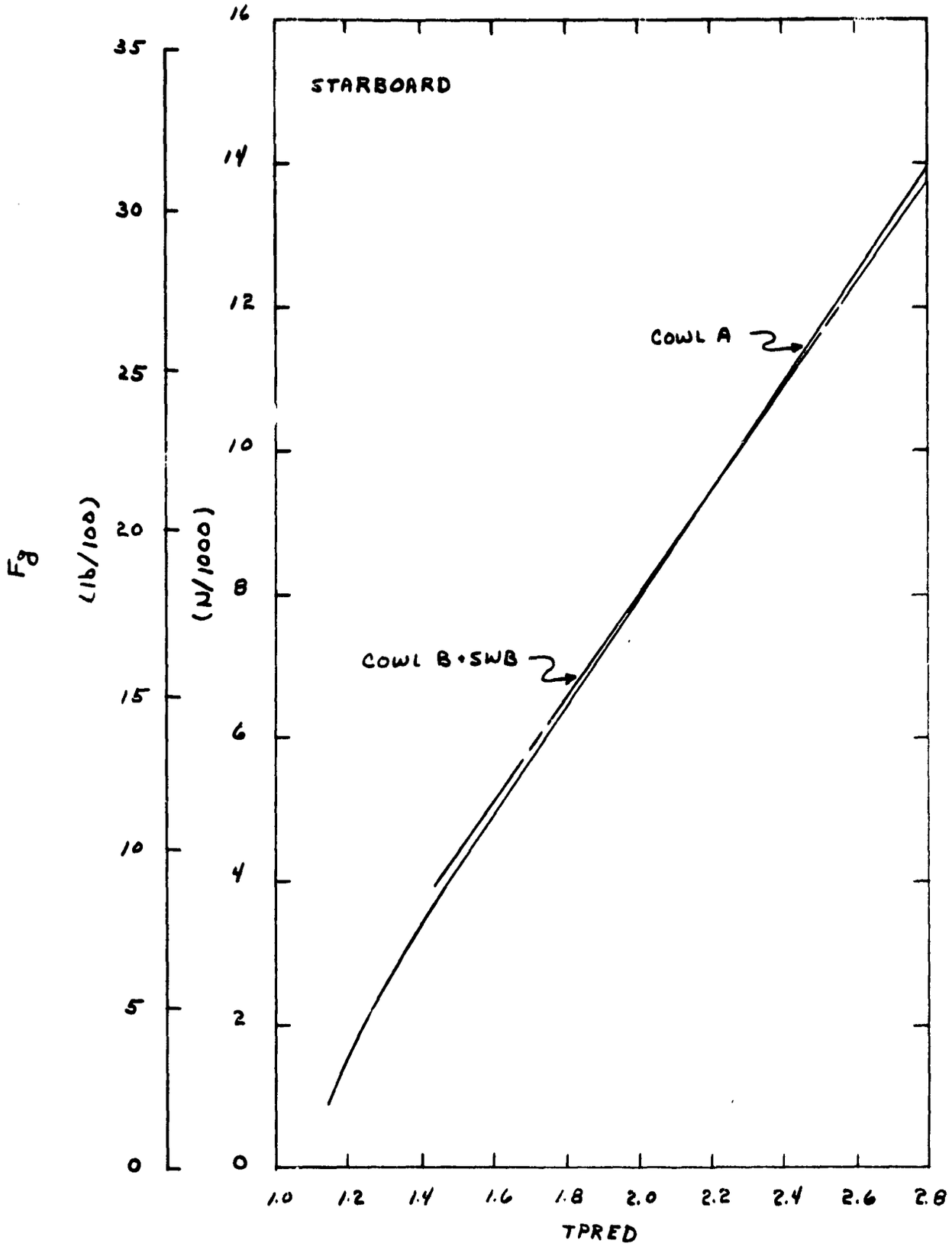

(b) STARBOARD ENGINE ONLY

FIGURE 6. CONCLUDED

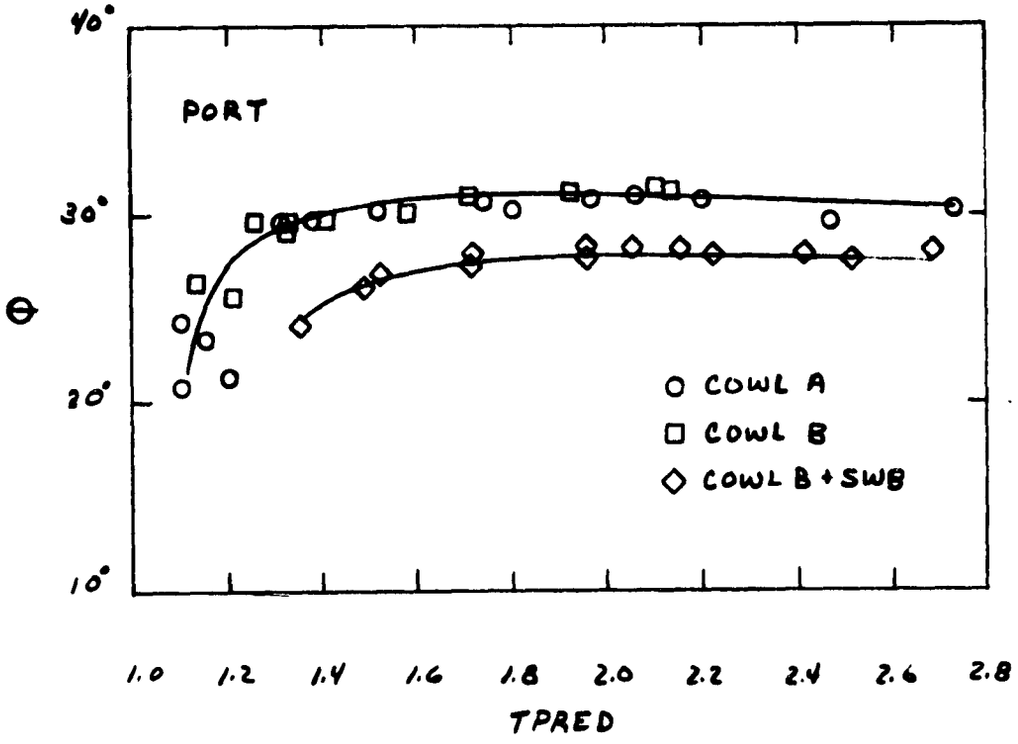

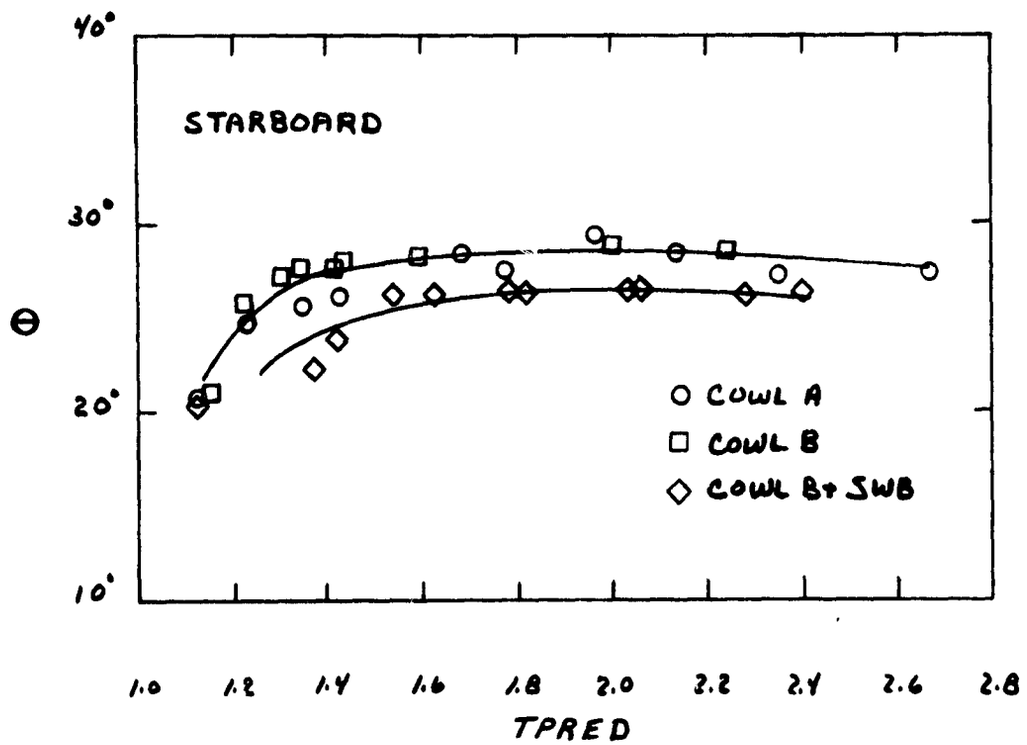

FIGURE 7. THRUST TURNING (NO FLAP)

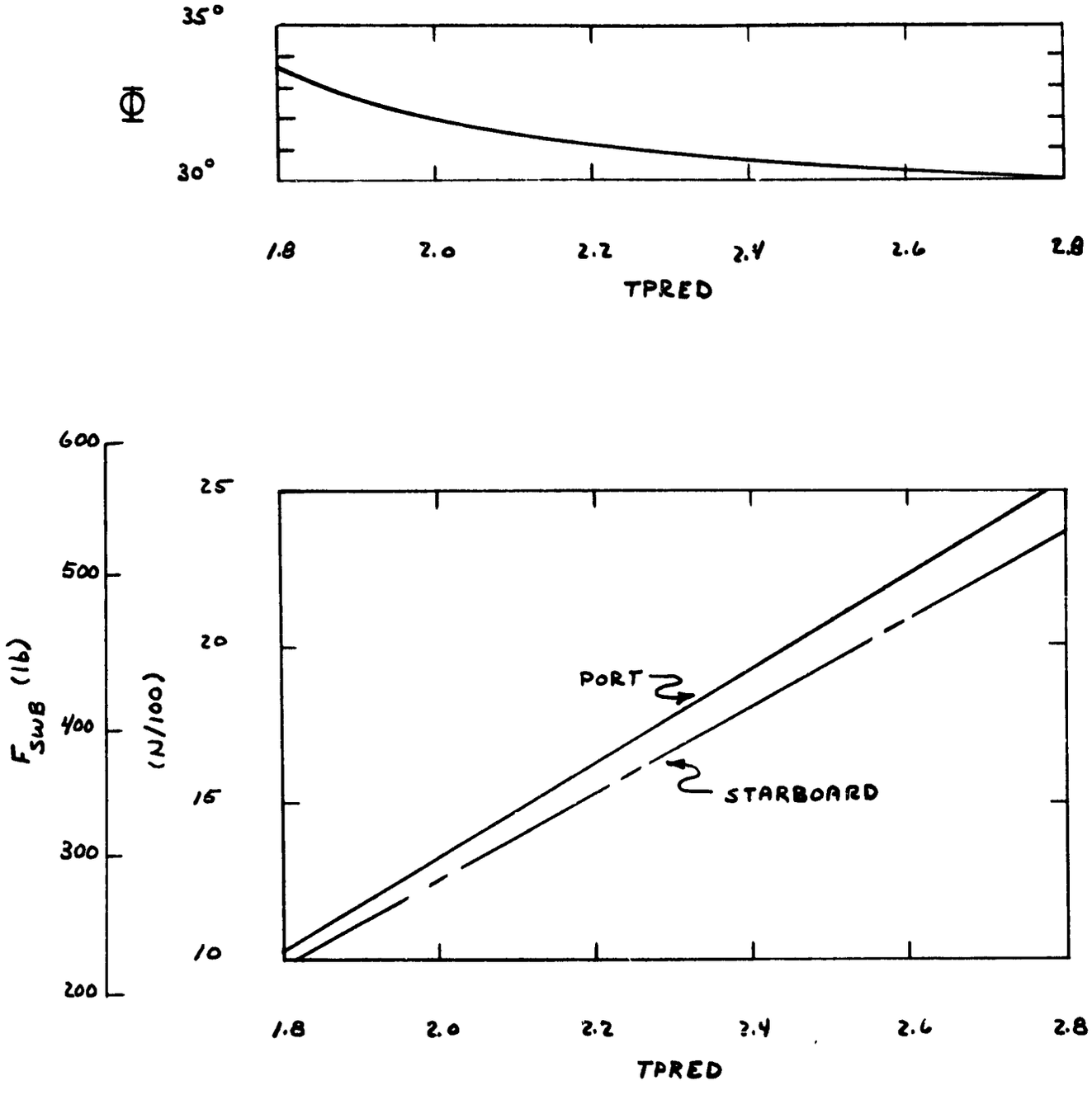

(a) SPANWISE BLOWING FORCE AND SWEEP

FIGURE 8. SPANWISE BLOWING

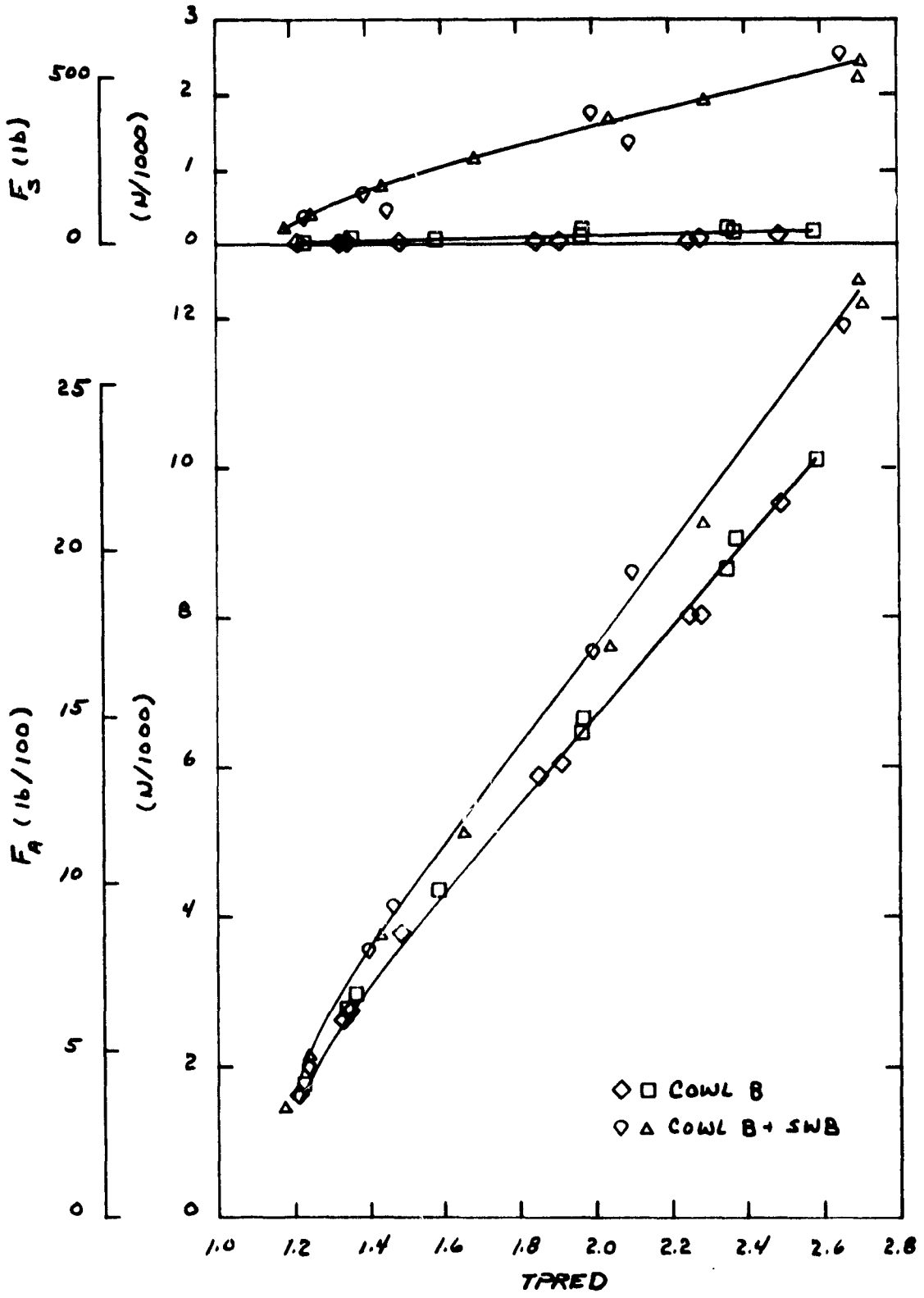

(b) CHANGE IN AXIAL AND SIDE FORCE DUE TO SWB

FIGURE 8. CONCLUDED

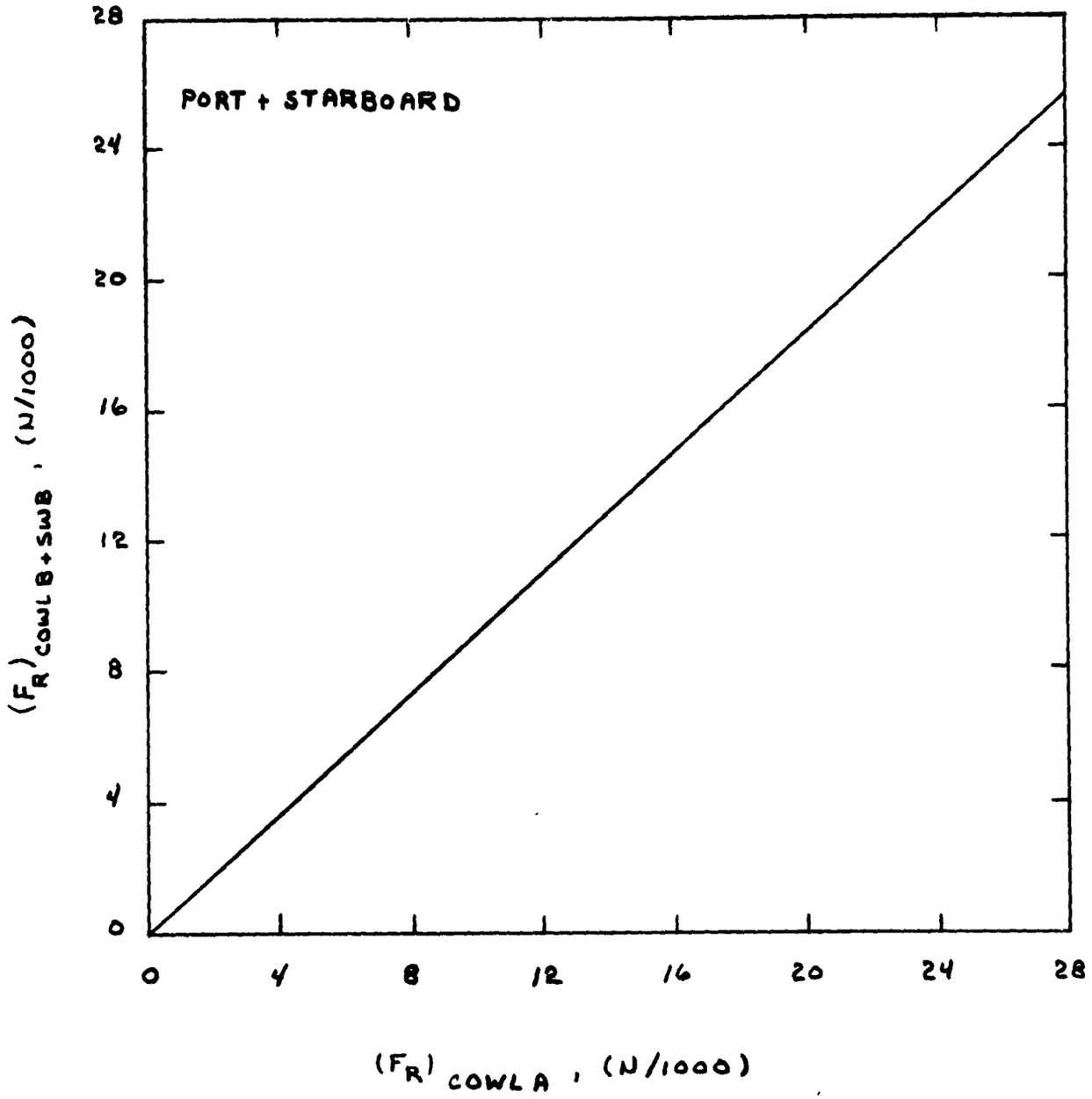

FIGURE 9. COMPARISON OF THE LONGITUDINAL RESULTANT THRUST PRODUCED BY EACH CONFIGURATION (NO FLAP)

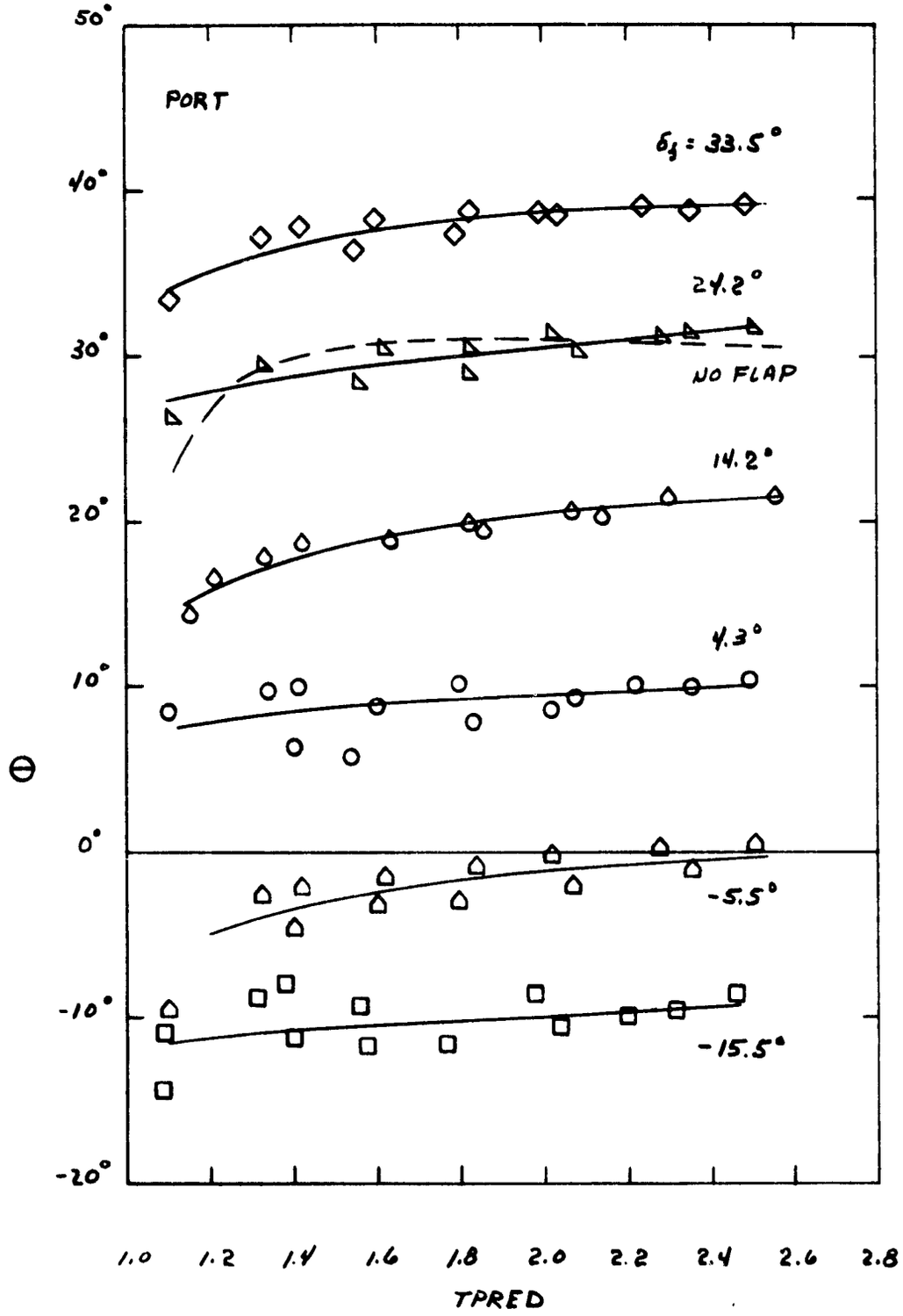

(a) THRUST TURNING - PORT ENGINE ONLY

FIGURE 10. EFFECT OF FLAP DEFLECTION

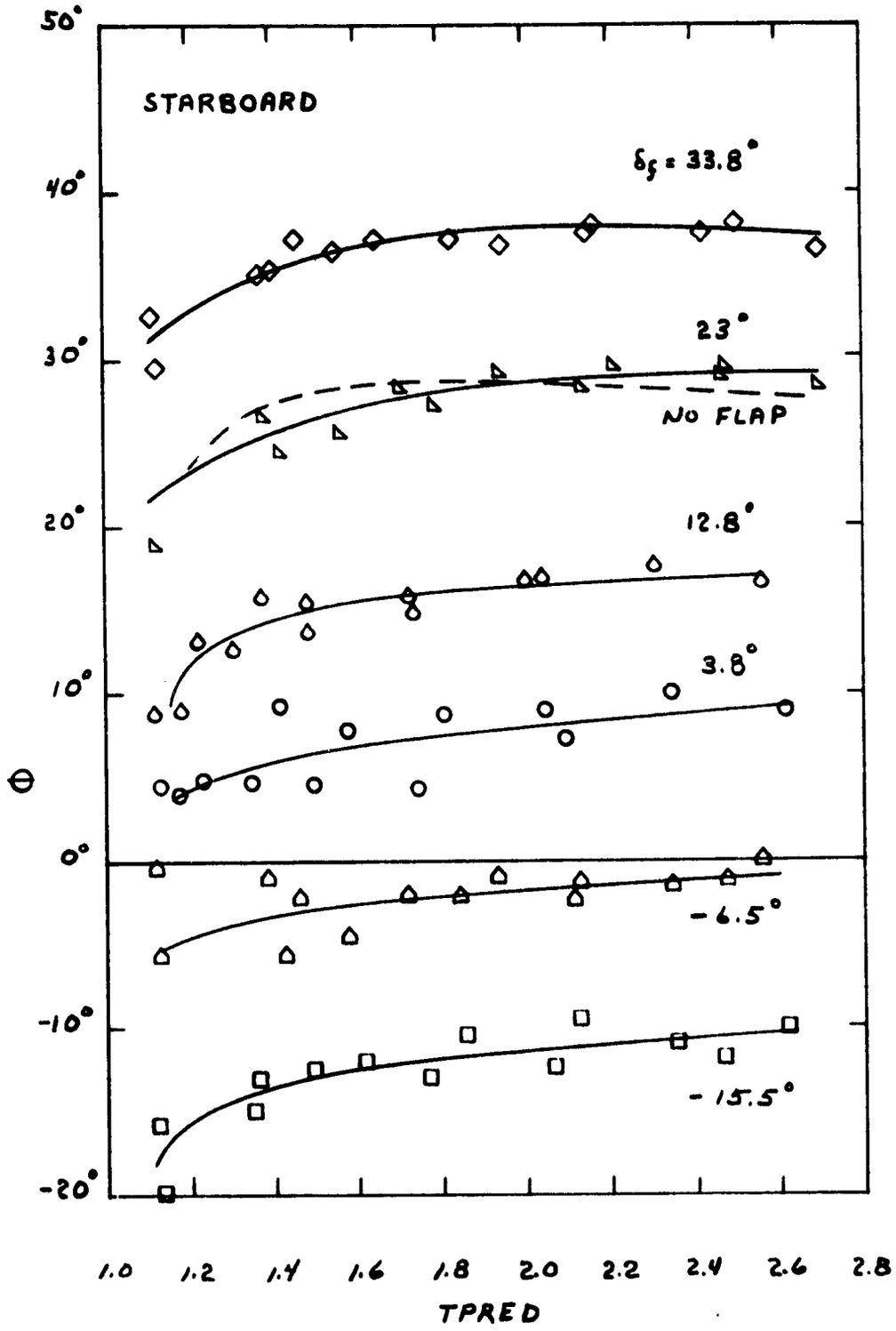

(b) THRUST TURNING - STARBOARD ENGINE ONLY

FIGURE 10. CONTINUES

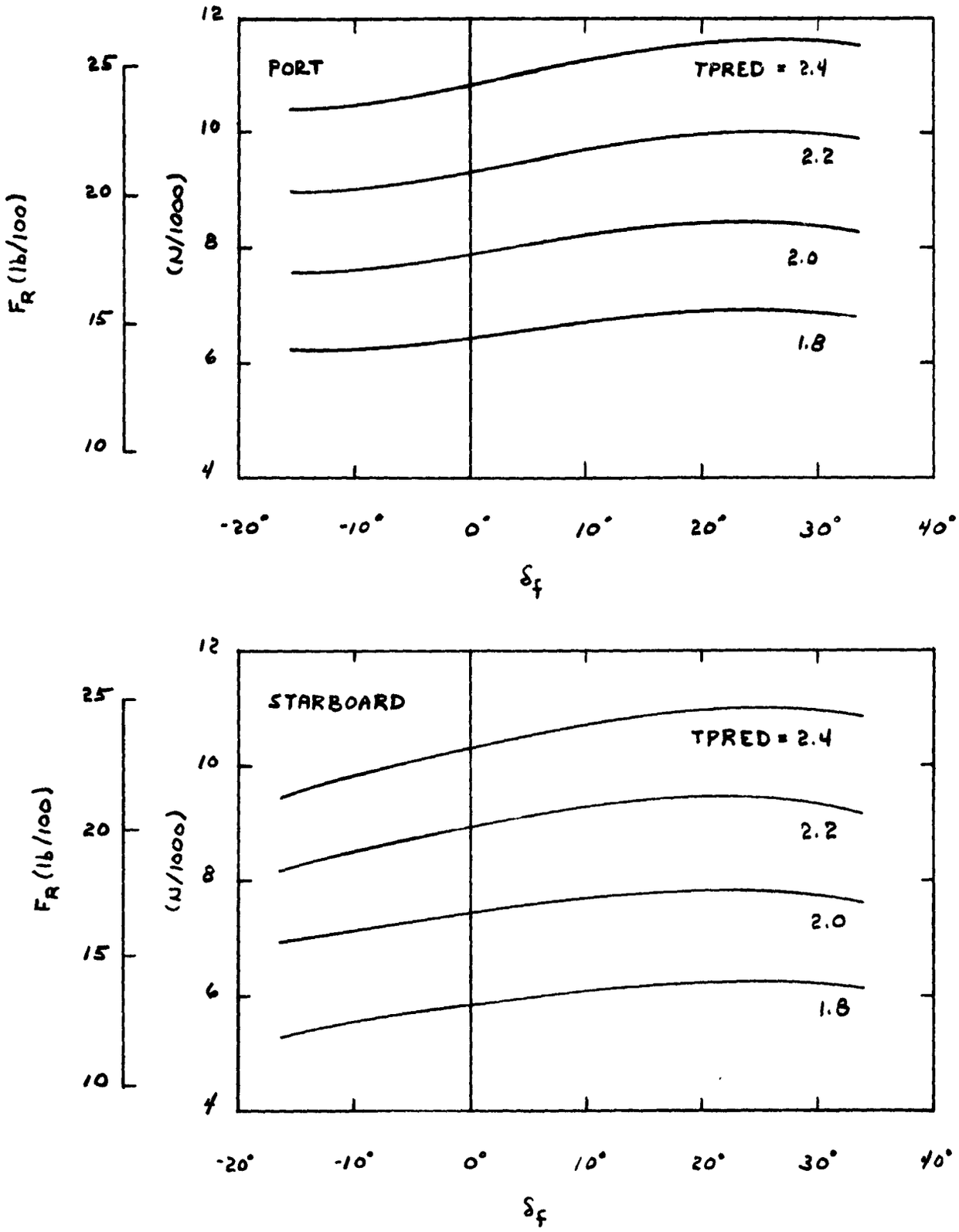

(C) FLAP ON RESULTANT THRUST

FIGURE 10. CONTINUES

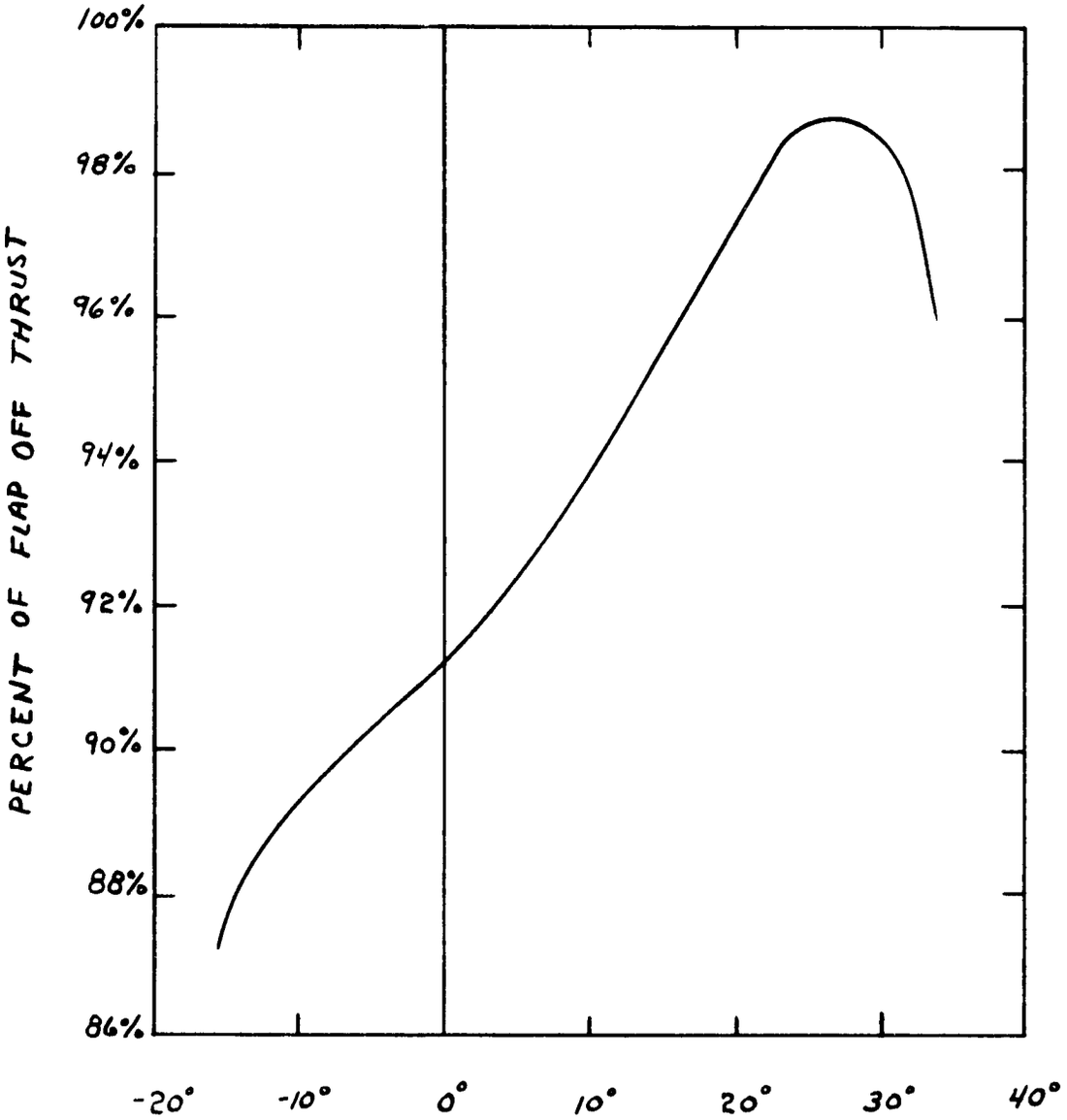

(d) AVERAGE THRUST LOSS DUE TO FLAP DEFLECTION

FIGURE 10. CONCLUDED

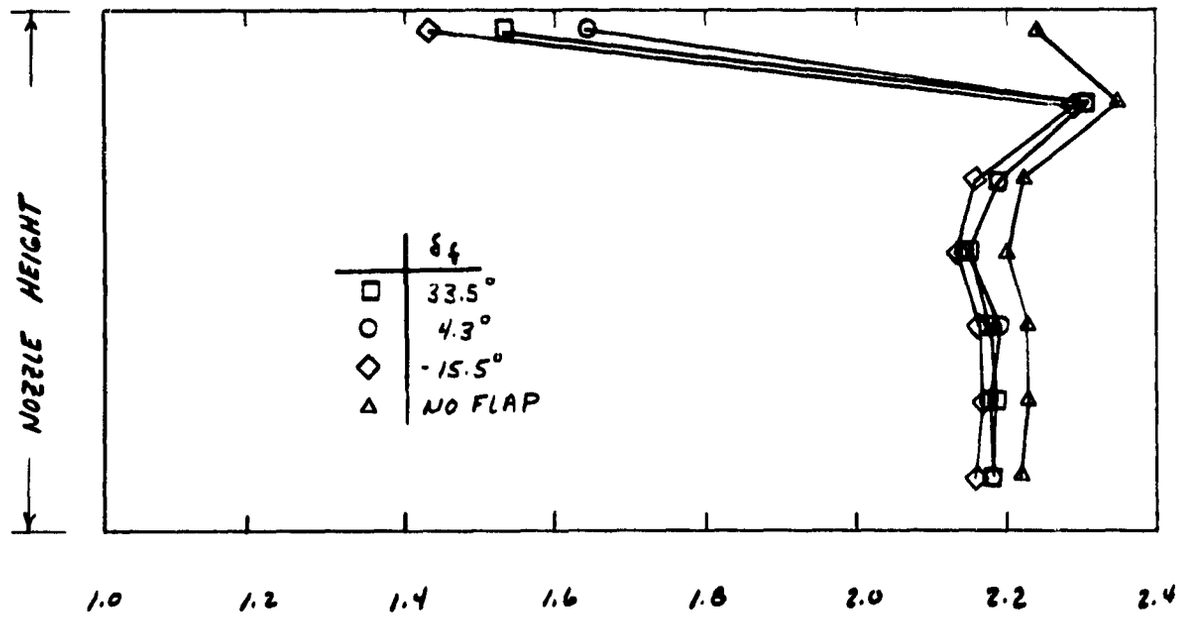

(a) NOZZLE RAKE PRESSURE PROFILE

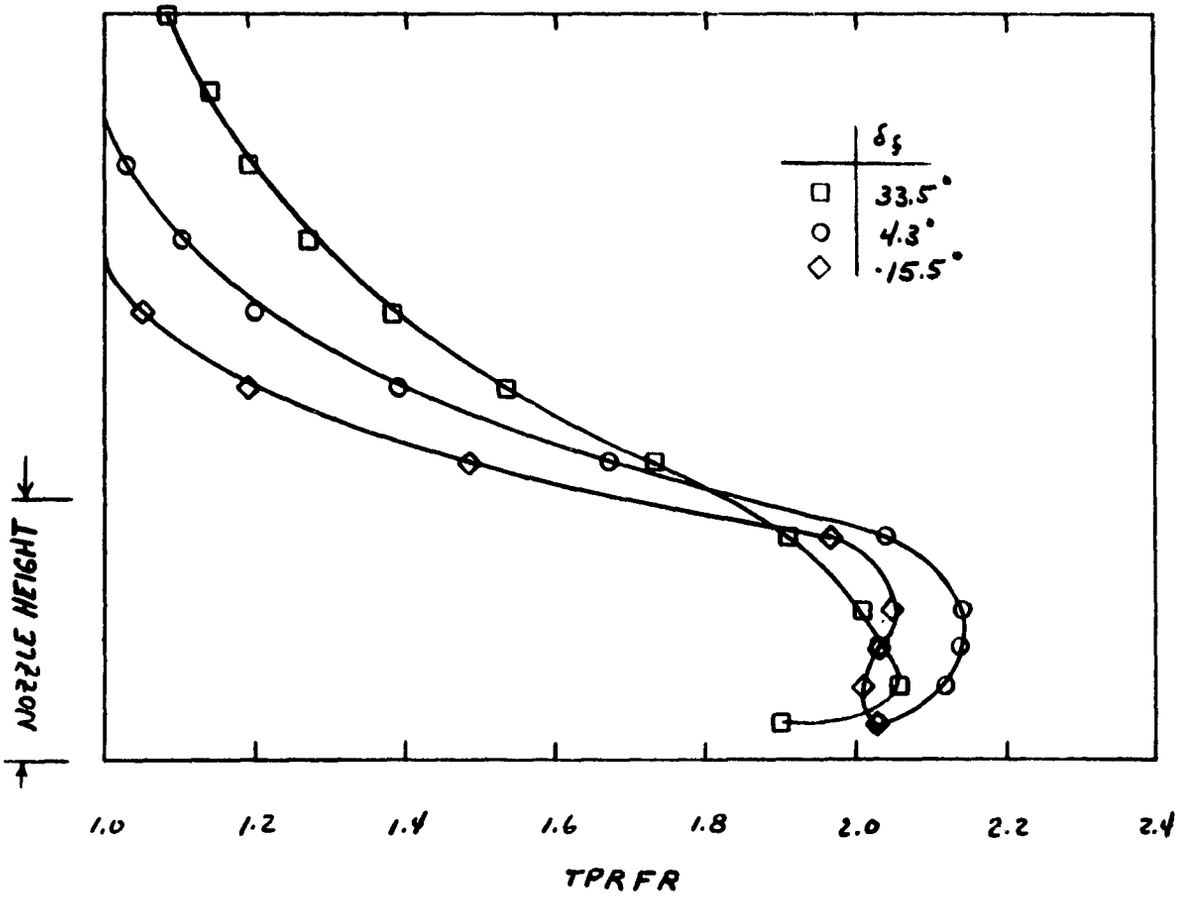

(b) FLAP RAKE PRESSURE PROFILE

FIGURE 11. EXHAUST JET PRESSURE PROFILE (TPRED = 2.5)

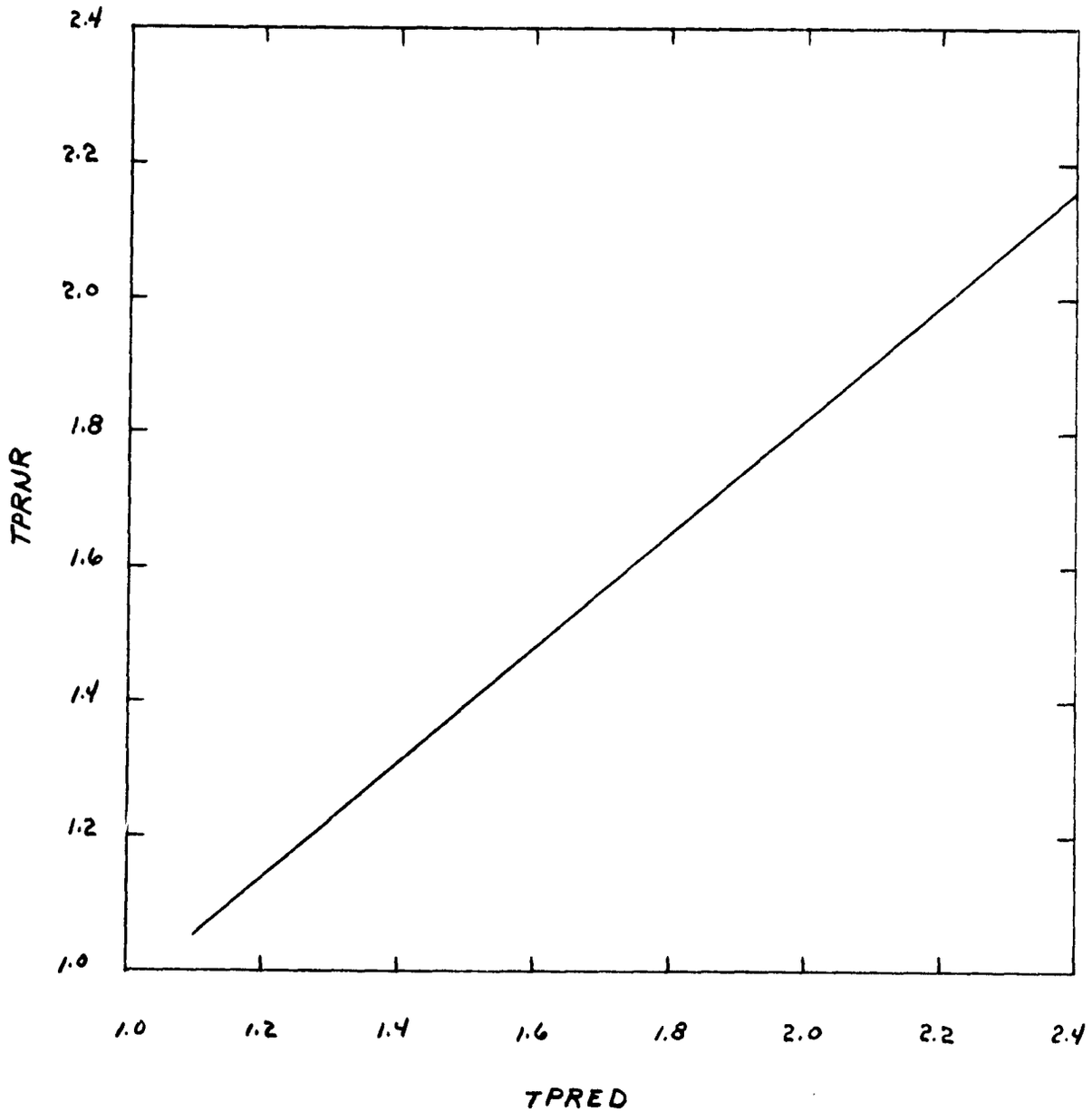

FIGURE 12. TOTAL PRESSURE LOSS THROUGH EXHAUST DUCT AND PRIMARY NOZZLE